Syntheses, Structures, and Physicochemical Properties of Diruthenium Compounds of Tetrachlorocatecholate with Metal−Metal Bonded $Ru^{3+}(\mu\text{-}OR)_2Ru^{3+}$ and $Ru^{3.5+}(\mu\text{-}OR)_2Ru^{3.5+}$ Cores (R = CH_3 and C_2H_5)

Hitoshi Miyasaka, Ho−Chol Chang, Katsunori Mochizuki, and Susumu Kitagawa*

Department of Synthetic Chemistry and Biological Chemistry, Faculty of Engineering, Kyoto University, Yoshida, Sakyo-ku, Kyoto 606-8501, Japan

Received September 8, 2000

Metal−metal bonded $Ru^{3+}(\mu\text{-}OR)_2Ru^{3+}$ and $Ru^{3.5+}(\mu\text{-}OR)_2Ru^{3.5+}$ (R = CH_3 and CH_3CH_2) compounds with tetrachlorocatecholate (Cl_4Cat) have been synthesized in the corresponding alcohol, MeOH and EtOH, from a nonbridged $Ru^{2+}-Ru^{3+}$ compound, $Na_3[Ru_2(Cl_4Cat)_4(THF)]\cdot 3H_2O\cdot 7THF$ (**1**). In alcohol solvents, compound **1** is continuously oxidized by oxygen to form $Ru^{3+}(\mu\text{-}OR)_2Ru^{3+}$ and $Ru^{3.5+}(\mu\text{-}OR)_2Ru^{3.5+}$ species. The presence of a characteristic countercation leads to selective isolation of either $Ru^{3+}(\mu\text{-}OR)_2Ru^{3+}$ or $Ru^{3.5+}(\mu\text{-}OR)_2Ru^{3.5+}$ as a stable adduct species. In methanol, Ph_4PCl and dibenzo-18-crown-6-ether afford $Ru^{3+}(\mu\text{-}OMe)_2Ru^{3+}$ species, $[A]_2[Ru_2(Cl_4Cat)_4(\mu\text{-}OMe)_2Na_2(MeOH)_6]$ ($[A]^+ = Ph_4P^+$ (**2**), $[Na(dibenzo\text{-}18\text{-}crown\text{-}6)(H_2O)(MeOH)]^+$ (**3**)), while benzo-15-crown-5-ether provides a $Ru^{3.5+}(\mu\text{-}OMe)_2Ru^{3.5+}$ species, $[Na(benzo\text{-}15\text{-}crown\text{-}5)_2][Ru_2(Cl_4Cat)_4(\mu\text{-}OMe)_2Na_2(MeOH)_6]$ (**4**). The air oxidation of **1** in a MeOH/EtOH mixed solvent (1:1 v/v) containing benzo-15-crown-5-ether provides a $Ru^{3.5+}(\mu\text{-}OMe)_2Ru^{3.5+}$ species, $[Na(benzo\text{-}15\text{-}crown\text{-}5)(H_2O)][Ru_2(Cl_4Cat)_2(\mu\text{-}OMe)_2Na_2(EtOH)_2(H_2O)_2(MeOH)_2]\cdot$(benzo-15-crown-5) (**5**). Similarly, the oxidation of **1** in ethanol with Ph_4PCl provides a $Ru^{3.5+}(\mu\text{-}OEt)_2Ru^{3.5+}$ species, $(Ph_4P)[Ru_2(Cl_4Cat)_4(\mu\text{-}OEt)_2Na_2(EtOH)_6]$ (**7**). A selective formation of a $Ru^{3+}(\mu\text{-}OEt)_2Ru^{3+}$ species, $(Ph_4P)_2[Ru_2(Cl_4Cat)_4(\mu\text{-}OEt)_2Na_2(EtOH)_2(H_2O)_2]$ (**6**), is found in the presence of pyrazine or 2,5-dimethylpyrazine. The crystal structures of these compounds, except **2** and **7**, have been determined by X-ray crystallography, and all compounds have been characterized by several spectroscopic and magnetic investigations. The longer Ru−Ru bonds are found in the $Ru^{3+}(\mu\text{-}OR)_2Ru^{3+}$ species (2.606(1) and 2.628(2) Å for **3** and **6**, respectively) compared with those of $Ru^{3.5+}(\mu\text{-}OMe)_2Ru^{3.5+}$ species (2.5260(6) Å and 2.514(2) Å for **4** and **5**, respectively). These structural features and magnetic and ESR data revealed the electronic configurations of $\sigma^2\pi^2\delta^{*2}\delta^2\pi^{*2}$ and $\sigma^2\pi^2\delta^{*2}\delta^2\pi^{*1}$ for $Ru^{3+}(\mu\text{-}OR)_2Ru^{3+}$ and $Ru^{3.5+}(\mu\text{-}OR)_2Ru^{3.5+}$, respectively, in which the former is diamagnetic and the latter is paramagnetic with $S = {}^1/_2$ ground state. Compound **5** forms a one-dimensional chain with alternating arrangement of a $Ru^{3.5+}(\mu\text{-}OMe)_2Ru^{3.5+}$ unit and a free benzo-15-crown-5-ether molecule by intermolecular hydrogen bonds ($O(H_2O)\cdots O(crown\text{-}ether) = 2.91-3.04$ Å). The cyclic voltammetry in DMF affords characteristic metal-origin voltammograms; two reversible and two quasi-reversible redox waves were observed. The feature of cyclic voltammograms for the $Ru^{3+}(\mu\text{-}OR)_2Ru^{3+}$ species (**2**, **3**, and **6**) and the $Ru^{3.5+}(\mu\text{-}OR)_2Ru^{3.5+}$ species (**4** and **7**) are similar to each other, indicating that both species are electrochemically stable. The isolation of the pyrazine-*trans*-coordinated species, $[Ph_4P][Ru(Cl_4Cat)_2(L)_2]$ (L = pyrazine (**8**), 2,5-dimethylpyrazine (**9**)), revealed the selective isolation of **6** from pyrazine-containing solution. UV−vis spectral variation by ethanolysis for **9** demonstrated the selective conversion from the pyrazine-*trans*-coordinated species to the $Ru^{3+}(\mu\text{-}OEt)_2Ru^{3+}$ species without an oxidation to the $Ru^{3.5+}(\mu\text{-}OEt)_2Ru^{3.5+}$ species. This result suggests the presence of equilibrium between $[Ru(Cl_4Cat)_2(L)_2]^-$ and $Ru^{3+}(\mu\text{-}OEt)_2Ru^{3+}$ species in the synthetic condition for **6**.

Introduction

Dinuclear ruthenium complexes with oxo (μ-O),[1−8] hydroxo (μ-OH),[9] and alkoxo (μ-OR) bridges[10] are of substantial interest in understanding the redox chemistry of polynuclear ruthenium cores because of not only the variety of geometric and electronic structures but also the catalytic reactivity for oxidation of water

(1) Gilbert, J. A.; Eggleston, D. S.; Murphy, W. R., Jr.; Geselowitz, D. A.; Gersten, S. W.; Hodgson, D. J.; Meyer, T. J. *J. Am. Chem. Soc.* **1985**, *107*, 3855.
(2) Schoonover, J. R.; Ni, J.; Roecher, L.; White, P. S.; Meyer, T. J. *Inorg. Chem.* **1996**, *35*, 5885.
(3) Phelps, D. W.; Kahn, E. M.; Hodgson, D. J. *Inorg. Chem.* **1975**, *14*, 2486.
(4) (a) Masuda, H.; Taga, T.; Osaki, K.; Sugimoto, H.; Mori, M.; Ogoshi, H. *Bull. Chem. Soc. Jpn.* **1982**, *55*, 3887. (b) Masuda, H.; Taga, T.; Osaki, K.; Sugimoto, H.; Mori, M.; Ogoshi, H. *J. Am. Chem. Soc.* **1981**, *103*, 2199.
(5) Schneider, R.; Weyhermüller, T.; Wieghardt, K. *Inorg. Chem.* **1993**, *32*, 4925.
(6) (a) Mathieson, A. McL.; Mellor, D. P.; Stephenson, N. C. *Acta Crystallogr.* **1952**, *5*, 185. (b) Deloume, J. P.; Faure, R.; Thomas-David, G. *Acta Crystallogr., Sect. B: Struct. Crystallogr. Cryst. Chem.* **1979**, *B35*, 558.
(7) Neubold, P.; Della Vedova, B. S. P. C.; Wieghardt, K.; Nuber, B.; Weiss, J. *Inorg. Chem.* **1990**, *29*, 3355.
(8) Power, J. M.; Evertz, K.; Henling, L.; Marsh, R.; Schaefer, W. P.; Labinger, J. A.; Bercaw, J. E. *Inorg. Chem.* **1990**, *29*, 5058.
(9) Kelson, E. P.; Henling, L. M.; Schaefer, W. P.; Labinger, J. A.; Bercaw, J. E. *Inorg. Chem.* **1993**, *32*, 2863.
(10) (a) Bardwell, D.; Jeffery, J. C.; Joulié, L.; Ward, M. D. *J. Chem. Soc., Dalton Trans.* **1993**, 2255. (b) Bardwell, D.; Horsburgh, L.; Jeffery, J. C.; Joulié, L.; Ward, M. D.; Webster, I.; Yellowlees, L. J. *J. Chem. Soc., Dalton Trans.* **1996**, 2527.

10.1021/ic0010252 CCC: $20.00
Published on Web 06/07/2001

and organic substrates. A series of mono-oxo-bridged diruthenium compounds (A) with 2,2′-bipyridine has been synthesized, and their catalytic mechanism for the oxidation of water has been energetically studied.[1−3,11−17] Regarding di-μ-oxo (B) and di-μ-hydroxo (C) diruthenium cores, several instances have been revealed by using an anionic tripod ligand, $[(\eta^5\text{-}C_5H_5)Co\{(CH_3O)_2P{=}O\}_3]^-$, where the homovalent series $Ru^{3+}(\mu\text{-}OH)_2Ru^{3+}$ of type (C) and $Ru^{4+}(\mu\text{-}O)_2Ru^{4+}$ and $Ru^{5+}(\mu\text{-}O)_2Ru^{5+}$ of type (B) were structurally characterized.[8,9]

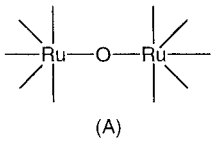

(A)

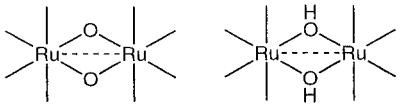

(B) (C)

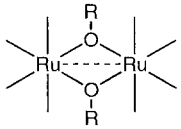

(D)

The isolation and characterization of each oxidation state in successive redox steps are necessary to understand and expand diruthenium chemistry. However, bridging cores of types B and C tend to undergo changes between themselves depending on solution conditions such as pH and oxidation states of ruthenium ions, making the $Ru(\mu\text{-}O)_2Ru$ core chemistry complicated. For the purpose we have focused on type D. To date only one sort of $Ru^{2+}(\mu\text{-}OR)_2Ru^{2+}$ compound (R = CH_3 and CH_3CH_2) has been reported by Ward et al.[10] Recently, we have synthesized a nonbridged diruthenium−tetrachlorocatecholate (Cl_4Cat) compound, $Na_3[Ru_2(Cl_4Cat)_4(THF)]\cdot 3H_2O\cdot 7THF$ (**1**), and its one-electron-oxidized compound, $Na_2[Ru_2(Cl_4Cat)_4(THF)_2]\cdot 3H_2O\cdot 3THF$.[18] Here, we wish to report that compound **1** is relevant to prepare a series of type D cores.

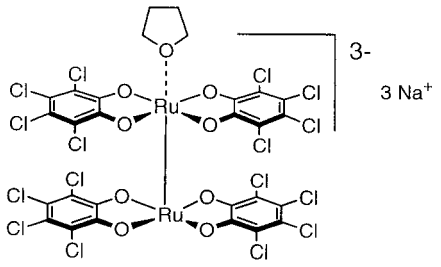

1

The oxidation products of **1** in MeOH and EtOH can be obtained as the corresponding $Ru^{3+}(\mu\text{-}OR)_2Ru^{3+}$ and $Ru^{3.5+}(\mu\text{-}OR)_2Ru^{3.5+}$ compounds by alcoholysis without an addition of any deprotonation reagents. We found the utility of sodium−crown ether complex and phosphonium cations for the isolation of these type D compounds: $Ru^{3+}(\mu\text{-}OMe)_2Ru^{3+}$ species, $[A]_2[Ru_2(Cl_4Cat)_4(\mu\text{-}OMe)_2Na_2(MeOH)_6]$ ($[A]^+ = Ph_4P^+$ (**2**), $[Na(dibenzo\text{-}18\text{-}crown\text{-}6)(H_2O)(MeOH)]^+$ (**3**)); $Ru^{3.5+}(\mu\text{-}OMe)_2Ru^{3.5+}$ species, $[Na(benzo\text{-}15\text{-}crown\text{-}5)_2][Ru_2(Cl_4Cat)_4(\mu\text{-}OMe)_2Na_2(MeOH)_6]$ (**4**) and $[Na(benzo\text{-}15\text{-}crown\text{-}5)(H_2O)][Ru_2(Cl_4Cat)_4(\mu\text{-}OMe)_2Na_2(EtOH)_2(H_2O)_2(MeOH)_2]\cdot$(benzo-15-crown-5) (**5**); $Ru^{3+}(\mu\text{-}OEt)_2Ru^{3+}$ species, $(Ph_4P)_2[Ru_2(Cl_4Cat)_4(\mu\text{-}OEt)_2Na_2(EtOH)_2(H_2O)_2]$ (**6**); and $Ru^{3.5+}(\mu\text{-}OEt)_2Ru^{3.5+}$ species, $(Ph_4P)[Ru_2(Cl_4Cat)_4(\mu\text{-}OEt)_2Na_2(EtOH)_6]$ (**7**). This paper describes their synthetic reactions, structural characterization, and physicochemical properties together with the characterization of the mononuclear ruthenium compounds, *trans*-$(Ph_4P)[Ru(Cl_4Cat)_2(L)_2]$ (L = pyrazine (**8**), 2,5-dimethylpyrazine (**9**)).

Results and Discussion

Syntheses and Isolations of 2−7. The equilibrium between the $Ru^{3+}(\mu\text{-}OMe)_2Ru^{3+}$ and $Ru^{3.5+}(\mu\text{-}OMe)_2Ru^{3.5+}$ species is established in MeOH, and either of those species, which is more stabilized by forming an ion pair with a characteristic countercation, is isolated selectively as a crystalline solid. An addition of Ph_4PCl affords a $Ru^{3+}(\mu\text{-}OMe)_2Ru^{3+}$ species, **2**, in which two Ph_4P^+ cations are involved. Sodium−crown-ether complexes sometimes become a good countercation for anionic assembly compounds, so we attempted the selective isolation of each species by using several crown-ether molecules; an addition of dibenzo-18-crown-6-ether affords a $Ru^{3+}(\mu\text{-}OMe)_2Ru^{3+}$ species of **3** with two $[Na(dibenzo\text{-}18\text{-}crown\text{-}6)(H_2O)(MeOH)]^+$ countercations. The choice of benzo-15-crown-5-ether affords a $Ru^{3.5+}(\mu\text{-}OMe)_2Ru^{3.5+}$ species of **4** containing one $[Na(benzo\text{-}15\text{-}crown\text{-}5)_2]^+$ countercation (Scheme 1). In a mixed solution of MeOH/EtOH, a $Ru^{3.5+}(\mu\text{-}OMe)_2Ru^{3.5+}$ species, **5**, is obtained as a salt with $[Na(benzo\text{-}15\text{-}crown\text{-}5)(H_2O)]^+$ similar to **4** (Scheme 2). A remarkable structural aspect of **5** is that a free benzo-15-crown-5-ether molecule contained in the crystal unit forms a 1-D hydrogen bonded chain with $Ru^{3.5+}(\mu\text{-}OMe)_2Ru^{3.5+}$ moieties (see structural description).

On the other hand, in EtOH, an addition of Ph_4PCl affords a $Ru^{3.5+}(\mu\text{-}OEt)_2Ru^{3.5+}$ species, **7**, as a salt with the Ph_4P^+ cation. The selective isolation of a $Ru^{3+}(\mu\text{-}OEt)_2Ru^{3+}$ species of **6** is successful when pyrazine or 2,5-dimethylpyrazine (more than 2 equiv per Ru) exists in solution (Scheme 3).

Structural Descriptions of Diruthenium Cores of $Ru^{3+}(\mu\text{-}OR)_2Ru^{3+}$ (3, R = Me; 6, R = Et) and $Ru^{3.5+}(\mu\text{-}OR)_2Ru^{3.5+}$ (4 and 5, R = Me). The formulated molecules of **3** and **6** consist of an anionic cluster and two countercations (two Na^+-dibenzo-18-crown-6-ether cations for **3** and two Ph_4P^+ cations for **6**). On the other hand, compounds **4** and **5** consist of an anionic cluster and one Na^+-benzo-15-crown-5-ether cation. It should be first mentioned that the structural features of the anionic moieties of all compounds are very similar to each other, except for **5** (vide infra), forming a Na_2Ru_2 double cuboidal cluster which is composed of two ruthenium ions bridged by two OMe or OEt ligands and two sodium ions as shown in Figure 1. The overall features of the anionic moieties of **3**−**5** are depicted in Figure 2 (**3** and **4**) and Figure 3 (**5**) (Figure S1 as Supporting Information, showing an ORTEP

(11) Weaver, T. R.; Meyer, T. J.; Adeyemi, S.; Brown, G. M.; Eckberg, R. P.; Hatfield, W. E.; Johnson, E. C.; Murray, R. W.; Untereker, D. *J. Am. Chem. Soc.* **1975**, *97*, 3039.
(12) Ikeda, M.; Shimizu, K.; Sato, G. P. *Bull. Chem. Soc. Jpn.* **1982**, *55*, 797.
(13) Doppelt, P.; Meyer, T. J. *Inorg. Chem.* **1987**, *26*, 2027.
(14) Geselowitz, D.; Meyer, T. J. *Inorg. Chem.* **1990**, *29*, 3894.
(15) Hurst, J. K.; Zhou, J.; Lei, Y. *Inorg. Chem.* **1992**, *31*, 1010
(16) Lei, Y.; Hurst, J. K. *Inorg. Chem.* **1994**, *33*, 4460.
(17) Lei, Y.; Hurst, J. K. *Inorg. Chim. Acta* **1994**, *226*, 179 and references therein.
(18) Kondo, M.; Hamatani, M.; Kitagawa, S.; Pierpont, C.; Unoura, K. *J. Am. Chem. Soc.* **1998**, *120*, 455.

Scheme 1

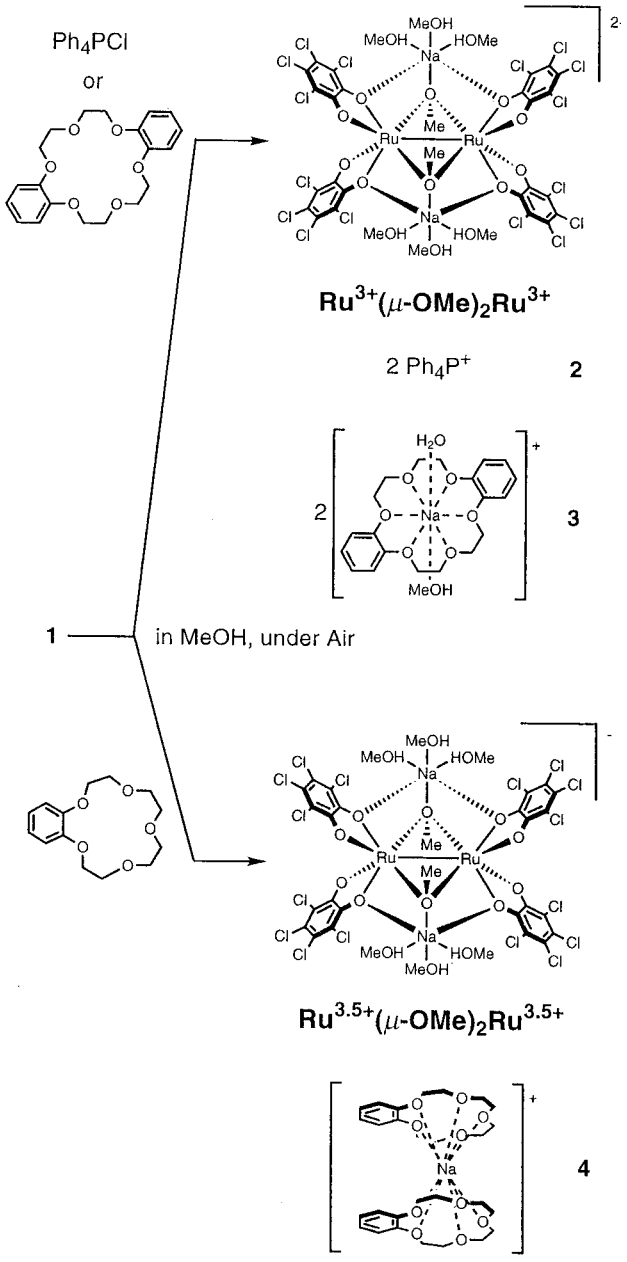

drawing of **6**). Selected bond distances and angles are listed in Tables 1−3, respectively. So, the descriptions for **3** and **4** are mainly described in details here. Each ruthenium ion is assumed to be in a pseudooctahedral coordination geometry, where two $Cl_4C_6O_2$ ligands and two OMe (OEt for **6**) ligands coordinate to each ruthenium ion in a cis-fashion. All $Cl_4C_6O_2$ ligands exhibit a catecholate form with the C−O distance in the range 1.28−1.35 Å. The Ru−O_{Cl4Cat} bonds are distinguishable as two groups, being in a position *trans* to the OMe bridging ligands and *perpendicular* to the OMe bridging ligands, where the former distance is shorter than the latter one. This trend is found in all compounds of **3**, **4**, **5**, and **6**. Two OMe groups for **3**−**5** and two OEt groups for **6** bridge Ru ions. For the bridging core of **3**, the bond distance of Ru(1)−O(3) = 2.035(4) Å and the bond angles of Ru(1)−O(3)−Ru(1′) = 79.6(2)° and O(3)−Ru(1)−O(3′) = 100.4(2)° are found. The bridging part of **4** is constructed with the Ru−O_{OMe} bond distances of Ru(1)−O(5) = 2.017(3) Å, Ru(1)−O(6) = 2.024(4) Å, Ru(2)−O(5) = 2.016(4) Å, and Ru(2)−O(6) = 2.018(3) Å and the bond angles

Scheme 2

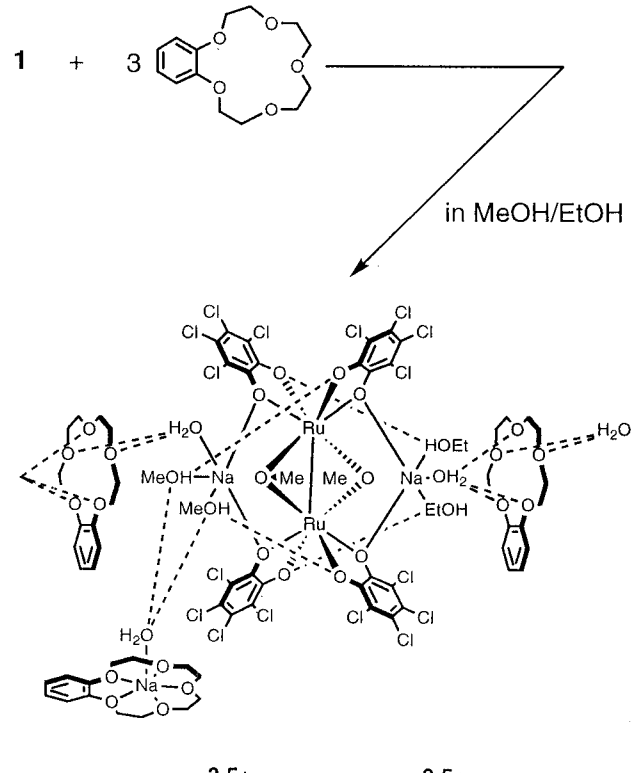

Ru(1)−O(5)−Ru(2) = 77.5(1)°, Ru(1)−O(6)−Ru(2) = 77.4(1)°, O(5)−Ru(1)−O(6) = 102.4(1)°, and O(5)−Ru(2)−O(6) = 102.7(1)°. The average Ru−O_{OMe} distance of **4**, 2.019 Å, is shorter than 2.035 Å of **3** (Δ = 0.016 Å). Interestingly, a notable difference in the diruthenium cores between **3** and **4** appears in the Ru−Ru bond. The Ru−Ru bond distance of **3** is 2.606(1) Å, which is compatible with that of $Ru^{3+}(\mu\text{-OEt})_2Ru^{3+}$ (**6**, 2.628(2) Å) and $Ru^{3+}(\mu\text{-OH})_2Ru^{3+}$ compounds reported previously.[9,19] On the other hand, the bond distance of **4** is 2.5260(6) Å, which is compatible with that of $Ru^{3.5+}(\mu\text{-OMe})_2Ru^{3.5+}$ (**5**, 2.514(2) Å) and $Ru^{3.5+}(\mu\text{-OH})_2Ru^{3.5+}$ compounds. [9] It is noteworthy that the Ru−Ru bond distances of $Ru^{3+}(\mu\text{-OR})_2Ru^{3+}$ species **3** and **6** are longer than those of $Ru^{3.5+}(\mu\text{-OMe})_2Ru^{3.5+}$ species **4** and **5** (Figure 1). The electronic configuration in a di-μ-bridging core having a metal−metal bond has been minutely investigated by Hoffmann et al.[19] and Cotton et al.[20,21] The electronic configurations for $Ru^{3+}(\mu\text{-OR})2Ru^{3+}$ and $Ru^{3.5+}(\mu\text{-OR})_2Ru^{3.5+}$ cores are interpreted to be $\sigma^2\pi^2\delta^{*2}\delta^2\pi^{*2}$ and $\sigma^2\pi^2\delta^{*2}\delta^2\pi^{*1}$, respectively.[8,9,19−21] The shorter Ru−Ru distances in **4** and **5** compared with those in **3** and **6** occur for electronic reasons rather than steric ones in the bridging core; the Ru−Ru bond order in the $Ru^{3+}(\mu\text{-OR})_2Ru^{3+}$ compounds **3** and **6** is 1.0 ($\sigma^2\pi^2\delta^{*2}\delta^2\pi^{*2}$), and, on the other hand, that in the $Ru^{3.5+}(\mu\text{-OR})_2Ru^{3.5+}$ compounds **4** and **5** is 1.5 ($\sigma^2\pi^2\delta^{*2}\delta^2\pi^{*1}$), which is caused by one-electron oxidation from an antibonding π^* orbital. The Ru−O_{OMe} distances also decrease in Δ = 0.016 Å from **3** to **4**: the average bond distances for **3** and **4** are 2.035 and 2.019 Å, respectively. Similarly a decrease

(19) Shaik, S.; Hoffmann, R.; Fisel, C. R.; Summervill, R. H. *J. Am. Chem. Soc.* **1980**, *102*, 4555.
(20) Cotton, F. A. *Polyhedron* **1987**, *6*, 667.
(21) Cotton, F. A.; Walton, R. A. *Multiple Bonds Between Metal Atoms*, 2nd ed.; Clarendon Press: Oxford, 1993.

Scheme 3

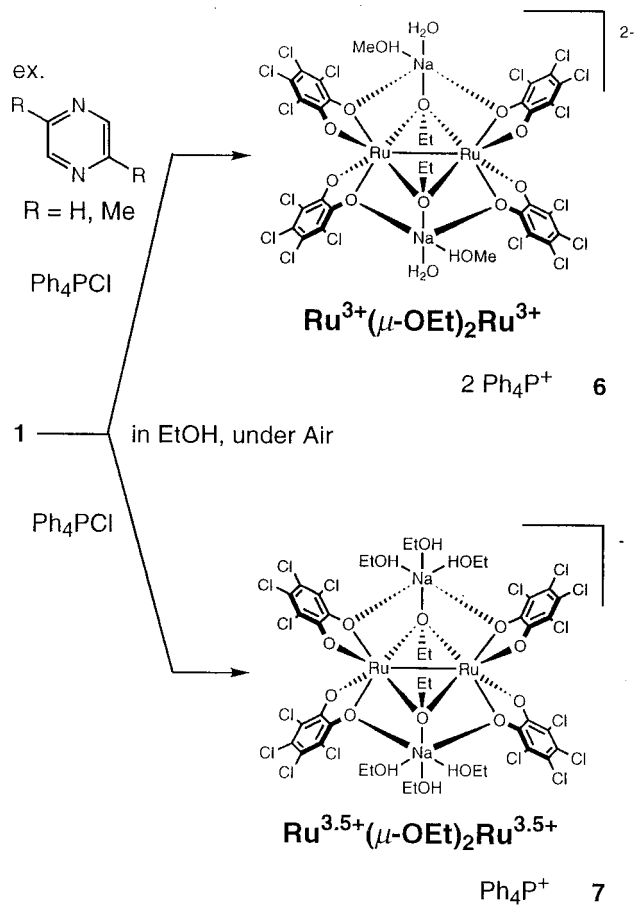

in the $Ru-O_{Cl4Cat}$ bond distances from **3** to **4** is observed. The deviations of $Ru-O_{Cl4Cat}$ bonds between **3** and **4** are $\Delta = 0.019$ Å for *trans*-$Ru-O_{Cl4Cat}$ and $\Delta = 0.038$ Å for *perpendicular*-$Ru-O_{Cl4Cat}$.

Each sodium ion has a O_6 coordination environment including two oxygen atoms of catecholates, three oxygen atoms of MeOH molecules, and one oxygen atom of a OMe bridging ligand. The overall bridging feature is assumed with a Na_2Ru_2 double cuboidal cluster (Figures 1 and 2), where the Na−catecholate and Na−OMe bonds constitute a part of the cuboidal skeleton. Two of three MeOH molecules coordinating to each sodium ion form an intramolecular hydrogen bond with catecholate oxygen atoms (dashed line in Figure 2).

Packing Description of $Ru^{3.5+}(\mu\text{-OMe})_2Ru^{3.5+}$ (5). Similarly to **3** and **4**, the cluster moiety of **5** consists of a ruthenium dinuclear trianion, $[(Cl_4Cat)_2Ru^{3.5+}(\mu\text{-OMe})_2Ru^{3.5+}(Cl_4Cat)_2]^{3-}$, and two sodium cations, where one water and two MeOH or two EtOH molecules coordinate to the sodium ions. The OMe bridging ligand does not interact with the sodium ion, the μ_2-bridging mode being dissimilar to the μ_3-bridging mode in **3** and **4** (Figure 1d). The MeOH and EtOH molecules coordinated to the sodium ions show intramolecular hydrogen bonds with catecholate oxygen atoms with bond distances of O(1)···O(10) = 2.80(2) Å and O(3)···O(8) = 2.84(2) Å (Figure 3). Interestingly, compound **5** forms a one-dimensional chain along the *b*-axis based on an intermolecular hydrogen bonding interaction between the coordinated water and the crown-ether oxygen atoms in the (2,3)-folding mode. The overview of an intermolecular hydrogen bonding chain is depicted in Figure 4. The intermolecular hydrogen bonds are observed as the bond distances of O(water)···O(ether) = 2.91(2), 2.94(3), and 3.04(2) Å. As mentioned above, the OMe bridging mode in **5** is a μ_2-bridging mode, while other compounds (**3**, **4**, and **6**) have a μ_3-bridging mode (Figure 1). The intermolecular hydrogen bonds prevent the coordination of Na ion to the OMe oxygen atom.

Spectral Characterization of 2−4, 6, and 7. Figure 5 shows UV−vis spectra of **3**, **4**, **6**, and **7** in MeCN under an N_2 atmosphere. The spectrum of **2** is essentially identical to that of **3**. The observed absorption parameters are summarized in Table 4. For **2** and **3**, the absorption bands at 474 nm (ϵ = 12600 $M^{-1}\cdot cm^{-1}$) and 470 nm (ϵ = 12600 $M^{-1}\cdot cm^{-1}$), respectively, are assigned to a Cat-to-Ru charge transfer (LMCT) band.[23] No other absorption bands are observed in the longer wavelength region. For **4**, three characteristic absorption bands at 575 nm (ϵ = 12800 $M^{-1}\cdot cm^{-1}$), 765 nm (ϵ = 6900 $M^{-1}\cdot cm^{-1}$), and 1400 nm (ϵ = 2500 $M^{-1}\cdot cm^{-1}$) are observed, in which the former two bands are assigned to Cat-to-Ru LMCT bands.[23] The broad weak absorption band at 1400 nm is observed only in the $Ru^{3.5+}(\mu\text{-OR})_2Ru^{3.5+}$ compounds of **4** and **7** (vide infra). Similar absorption bands have been found in previously reported dinuclear compounds in which two metal centers are supported by μ-oxo or μ-alkoxo bridges without direct metal−metal bonds: $[Ru_2(dtne)(\mu\text{-O})_2(\mu\text{-CO}_3)]PF_6\cdot 5H_2O$ (dtne = 1,2-bis(1,4,7-triazacyclononan-1-yl)ethane) with a $Ru^{3.5+}(\mu\text{-O})_2Ru^{3.5+}$ core shows a band at 1224 nm (ϵ = 406 $M^{-1}\cdot cm^{-1}$),[22] while the electrochemically generated $[Ru^{2.5+}(bpy)_2(\mu\text{-OMe})_2Ru^{2.5+}(bpy)_2]^{3+}$ (bpy = 2,2′-bipyridine) cation also demonstrates the absorption band at 1750 nm (ϵ = 5000 $M^{-1}\cdot cm^{-1}$) which was not detected in the homovalent compounds, $[Ru^{2+}(bpy)_2(\mu\text{-OMe})_2Ru^{2+}(bpy)_2]^{2+}$ and $[Ru^{3+}(bpy)_2(\mu\text{-OMe})_2Ru^{3+}(bpy)_2]^{4+}$.[10b] Ward et al. assigned this absorption band to a $\pi-\pi^*$ transition, which is associated with orbitals fully electron delocalized over $Ru_2(\mu\text{-OMe})_2$ core (class III characteristic), rather than a valence-localized class II species.[10b] In the case of **4** and **7**, the lower energy absorption band is also associated with a $Ru_2(\mu\text{-OR})_2$ core, attributable to an electronic transition based on principal d-orbital contribution for ruthenium ions because of the direct metal−metal bond system. The spectral features of **6** and **7** are essentially identical to those of **3** and **4**, respectively (see Table 4).

IR Spectral Studies. The dioxolene ligand in metal complexes has been well characterized by IR spectroscopy, in particular, the C−O stretching frequencies being characteristic of the oxidation state. In all of **2**−**7**, the bands are observed at ca. 1250 cm^{-1} (C−O stretching) and ca. 1420 cm^{-1} (ring breathing), indicative of the catecholate form (Table 4). If the semiquinonate species exists, the C−O stretching appear in the region of 1400−1500 cm^{-1}.[23f] Since all dioxolene ligands in **2**−**7** are the catecholate form, consequently, the valence of ruthenium ions is $Ru^{3+}(\mu\text{-OR})_2Ru^{3+}$ for **2**, **3**, and **6** and $Ru^{3.5+}(\mu\text{-OR})_2Ru^{3.5+}$ for **4**, **5**, and **7**, being compatible with the results obtained from the structural aspects.

(22) Geilenkirchen, A.; Neubold, P.; Schneider, R.; Wieghardt, K.; Flörke, U.; Haupt, H.-J.; Nuber, B. *J. Chem. Soc., Dalton Trans.* **1994**, 457.
(23) (a) Bhattacharya, S.; Boone, S. R.; Fox, G. A.; Pierpont, C. *J. Am. Chem. Soc.* **1990**, *112*, 1088. (b) Bhattacharya, S.; Pierpont, C. *Inorg. Chem.* **1994**, *33*, 6038. (c) Bhattacharya, S.; Pierpont, C. *Inorg. Chem.* **1991**, *30*, 1511. (d) Haga, M.; Dodsworth, E. S.; Lever, A. B. P.; Boone, S. R.; Pierpont, C. *J. Am. Chem. Soc.* **1986**, *108*, 7413. (e) Boone, S. R.; Pierpont, C. *Inorg. Chem.* **1987**, *26*, 1769. (f) Lever, A. B. P.; Auburn, P. R.; Dodsworth, E. S.; Haga, M.; Liu, W.; Melnik, M.; Nevin, A. *J. Am. Chem. Soc.* **1988**, *110*, 8076. (g) Haga, M.; Dodsworth, E. S.; Lever, A. B. P. *Inorg. Chem.* **1986**, *25*, 447. (h) Auburn, P. R.; Dodsworth, E. S.; Haga, M.; Liu, W.; Nevin, W. A.; Lever, A. B. P. *Inorg. Chem.* **1991**, *30*, 3502. (i) Masui, H.; Lever, A. B. P.; Auburn, P. R. *Inorg. Chem.* **1991**, *30*, 2402. (j) Boone, S. R.; Pierpont, C. G. *Polyhedron* **1990**, *9*, 2267.

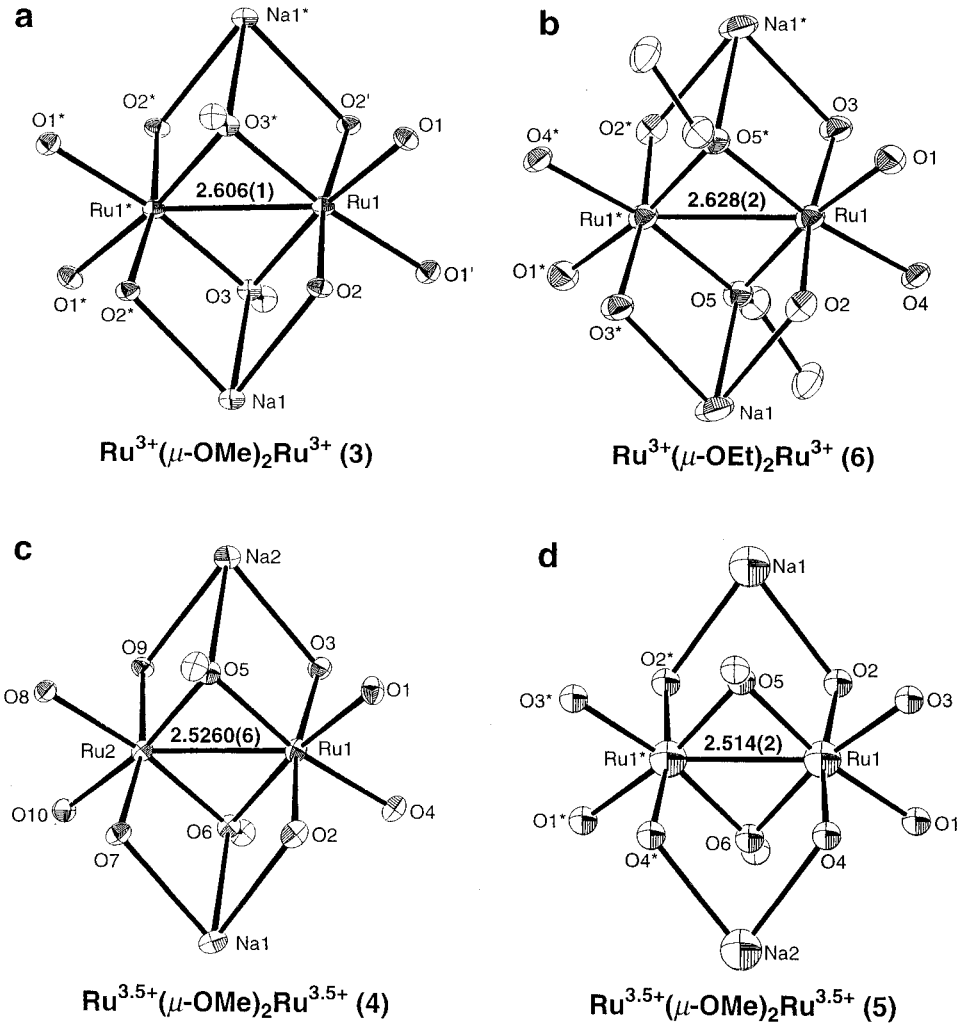

Figure 1. Coordination geometries of the Na_2Ru_2 cluster cores in (a) **3**, (b) **4**, (c) **5**, and (d) **6**, where **3** and **6** are classified into $Ru^{3+}(\mu\text{-}OR)_2Ru^{3+}$ species and **4** and **5** are classified into $Ru^{3.5+}(\mu\text{-}OMe)_2Ru^{3.5+}$ species.

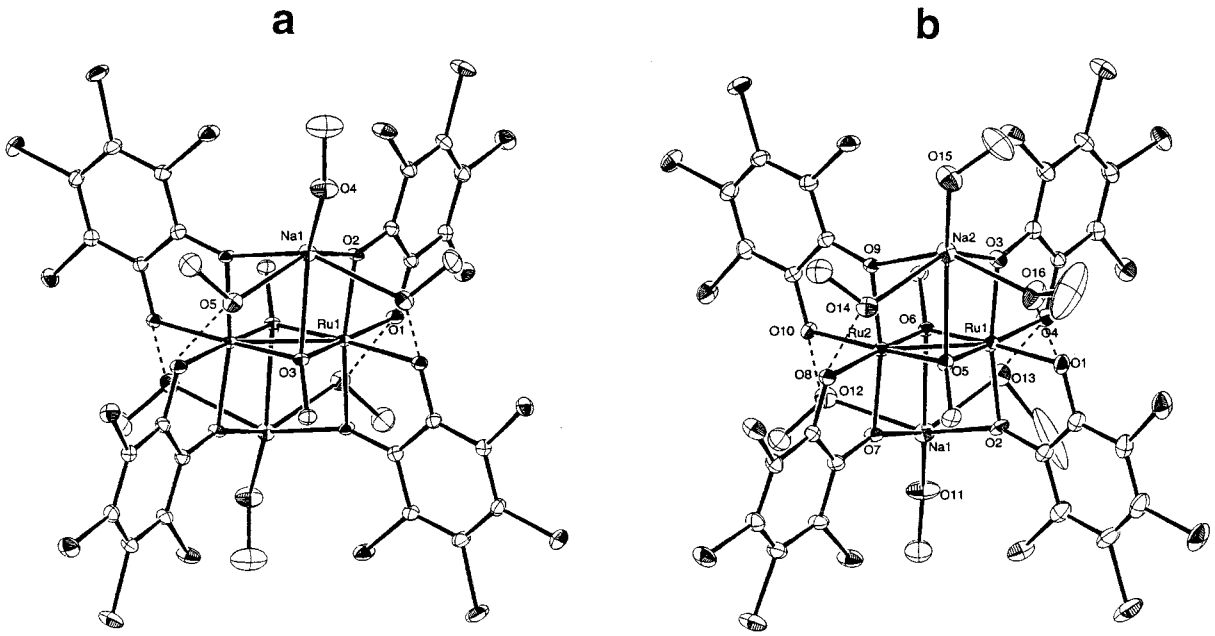

Figure 2. ORTEP drawings of the anionic moieties of (a) **3** and (b) **4**. The dashed lines denote hydrogen bond links. Hydrogen atoms are omitted for clarity.

Magnetic and ESR Studies. The temperature dependence of the magnetic susceptibilities for all compounds was measured between 1.9 and 300 K, and ESR spectra were recorded at 77 K for **4**, **5**, and **7**. The magnetic and ESR data for **2**−**7** are

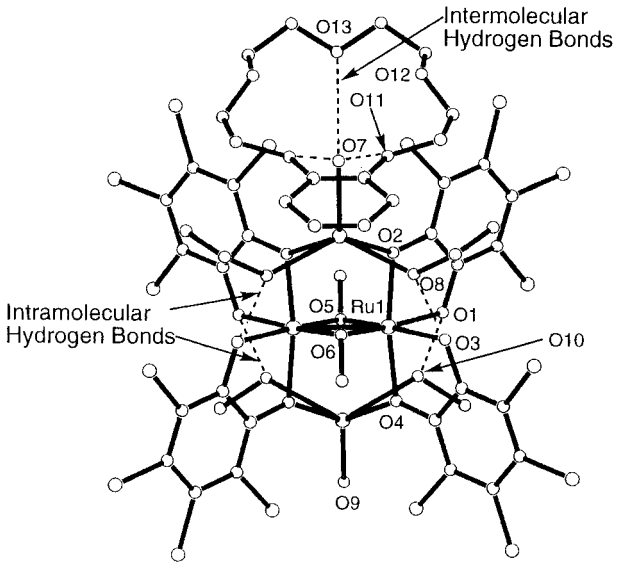

Figure 3. (a) Perspective view of the Na_2Ru_2 monoanionic cluster and free benzo-15-crown-5-ether molecule of **5**. (b) Intermolecular hydrogen bonding mode between Na_2Ru_2 anionic cluster and free benzo-15-crown-5-ether molecules, showing (2,3)-holding mode, where each hydrogen bond distance is given in Table 3.

Table 1. Relevant Bond Distances (Å) and Angles (deg) for **3** with the Estimated Standard Deviations in Parentheses[a]

Ru(1)−O(1)	2.016(4)	Na(1)−O(2)	2.308(4)
Ru(1)−O(2)	2.066(3)	Na(1)−O(3)	2.586(6)
Ru(1)−O(3)	2.035(4)	Na(1)−O(4)	2.372(7)
Ru(1)−Ru(1)*	2.606(1)	Na(1)−O(5)	2.506(4)
O(1)−Ru(1)−O(1)**	87.8(2)	O(2)−Ru(1)−O(2)**	170.4(2)
O(1)−Ru(1)−O(2)	83.2(1)	O(2)−Ru(1)−O(3)	91.7(2)
O(1)−Ru(1)−O(2)**	89.9(1)	O(2)−Ru(1)−O(3)*	94.4(2)
O(1)−Ru(1)−O(3)	172.0(1)	O(3)−Ru(1)−O(3)*	100.4(2)
O(1)−Ru(1)−O(3)*	86.1(1)	Ru(1)−O(3)−Ru(1)*	79.6(2)
Hydrogen Bonds			
O(1)···O(5)	2.730(5)		

[a] Symmetry operations: (*) $1-x, 1-y, 1-z$; (**) $1-x, y, 1-z$.

summarized in Table 4. Compounds **2**, **3**, and **6** are exactly diamagnetic. For **4**, the magnetic moments between 2.04 μ_B at 300 and 1.71 μ_B at 1.9 K, per dinuclear unit, clearly demonstrate a $S = {}^1/_2$ ground state. This magnetic data is compatible with the ESR spectrum of a powdered sample recorded at 77 K as shown in Figure 6a. The ESR signal displays a rhombic g value pattern with $g_1 = 2.54$, $g_2 = 2.01$, and $g_3 = 1.80$, which is consistent with those of $Ru^{3.5+}(\mu\text{-}O)_2Ru^{3.5+}$ compounds having a Ru−Ru bond reported previously.[22] The magnetic behavior for **5** is essentially the same as that of **4**, demonstrating a $S = {}^1/_2$ ground state (1.75 μ_B at 1.9 K and 2.02 μ_B at 300 K), and no apparent interdimer interaction was detected through the hydrogen bonds. The ESR spectrum of a powder sample of **5** is shown in Figure 6b, in which the signal pattern is more complicated than that of **4**, but similar in rhombic pattern. For **7**, the effective magnetic moment is 1.30 μ_B at 1.9 K and 1.72 μ_B at 300 K. The value of μ_{eff} at room temperature is slightly smaller than the values observed for **4** and **5** and the previously reported values (1.9−2.70 μ_B).[9,22] This is because the presence of a small amount of $Ru^{3+}(\mu\text{-}OEt)_2Ru^{3+}$ diamagnetic species could cause a slight deviation from the expected one. The g values are also consistent with the results from the $S = {}^1/_2$ ground state for $Ru^{3.5+}(\mu\text{-}OMe)_2Ru^{3.5+}$ species, where a rhombic signal with g values at $g_1 = 2.43$, $g_2 = 2.04$, and $g_3 = 1.86$ was observed (Figure 6c). These magnetic data, in addition to structural characterization, well demonstrate the electronic configurations $\sigma^2\pi^2\delta^{*2}\delta^2\pi^{*2}$ and $\sigma^2\pi^2\delta^{*2}\delta^2\pi^{*1}$ for $Ru^{3+}(\mu\text{-}OR)_2Ru^{3+}$ and $Ru^{3.5+}(\mu\text{-}OR)_2Ru^{3.5+}$, respectively, where the former is diamagnetic and the latter is paramagnetic with a $S = {}^1/_2$ ground state.

Table 2. Relevant Bond Distances (Å) and Angles (deg) for **4** with the Estimated Standard Deviations in Parentheses

Ru(1)−O(1)	2.001(4)	Na(1)−O(2)	2.398(4)
Ru(1)−O(2)	2.028(3)	Na(1)−O(6)	2.554(4)
Ru(1)−O(3)	2.020(3)	Na(1)−O(7)	2.377(4)
Ru(1)−O(4)	1.999(3)	Na(1)−O(11)	2.338(5)
Ru(1)−O(5)	2.017(3)	Na(1)−O(12)	2.458(5)
Ru(1)−O(6)	2.024(4)	Na(1)−O(13)	2.536(4)
Ru(2)−O(5)	2.016(4)	Na(2)−O(3)	2.371(4)
Ru(2)−O(6)	2.018(3)	Na(2)−O(5)	2.689(4)
Ru(2)−O(7)	2.031(3)	Na(2)−O(9)	2.401(4)
Ru(2)−O(8)	1.998(3)	Na(2)−O(14)	2.531(4)
Ru(2)−O(9)	2.032(3)	Na(2)−O(15)	2.323(5)
Ru(2)−O(10)	1.990(4)	Na(2)−O(16)	2.358(5)
Ru(1)−Ru(2)	2.5260(6)		
O(1)−Ru(1)−O(2)	83.4(2)	O(5)−Ru(2)−O(6)	102.7(1)
O(1)−Ru(1)−O(3)	90.1(1)	O(5)−Ru(2)−O(7)	96.6(1)
O(1)−Ru(1)−O(4)	87.7(1)	O(5)−Ru(2)−O(8)	84.5(1)
O(1)−Ru(1)−O(5)	84.9(1)	O(5)−Ru(2)−O(9)	90.2(1)
O(1)−Ru(1)−O(6)	170.8(1)	O(5)−Ru(2)−O(10)	170.4(1)
O(2)−Ru(1)−O(3)	169.7(1)	O(6)−Ru(2)−O(7)	90.1(1)
O(2)−Ru(1)−O(4)	88.2(1)	O(6)−Ru(2)−O(8)	170.7(1)
O(2)−Ru(1)−O(5)	97.7(1)	O(6)−Ru(2)−O(9)	96.5(1)
O(2)−Ru(1)−O(6)	90.1(1)	O(6)−Ru(2)−O(10)	85.1(1)
O(3)−Ru(1)−O(4)	83.5(1)	O(7)−Ru(2)−O(8)	83.2(1)
O(3)−Ru(1)−O(5)	89.6(1)	O(7)−Ru(2)−O(9)	169.3(1)
O(3)−Ru(1)−O(6)	95.4(1)	O(7)−Ru(2)−O(10)	88.8(1)
O(4)−Ru(1)−O(5)	169.9(1)	O(8)−Ru(2)−O(9)	89.2(1)
O(4)−Ru(1)−O(6)	85.6(1)	O(8)−Ru(2)−O(10)	88.3(1)
O(5)−Ru(1)−O(6)	102.4(1)	O(9)−Ru(2)−O(10)	83.4(1)
		Ru(1)−O(5)−Ru(2)	77.5(1)
		Ru(1)−O(6)−Ru(2)	77.4(1)
Hydrogen Bonds			
O(1)···O(16)	2.878(6)	O(4)···O(13)	2.763(6)
O(8)···O(14)	2.777(5)	O(10)···O(12)	2.756(5)

Table 3. Relevant Bond Distances (Å), Hydrogen Bond Distances (Å), and Angles (deg) for **5** with the Estimated Standard Deviations in Parentheses[a]

Ru(1)−O(1)	2.00(1)	Na(1)−O(2)	2.42(1)
Ru(1)−O(2)	2.03(1)	Na(1)−O(7)	2.36(2)
Ru(1)−O(3)	1.99(1)	Na(1)−O(8)	2.43(1)
Ru(1)−O(4)	2.021(10)	Na(2)−O(4)	2.37(1)
Ru(1)−O(5)	2.00(1)	Na(2)−O(9)	2.31(2)
Ru(1)−O(6)	2.02(1)	Na(2)−O(10)	2.62(1)
Ru(1)−Ru(1)*	2.514(2)		
O(1)−Ru(1)−O(2)	83.6(4)	O(3)−Ru(1)−O(4)	83.2(4)
O(1)−Ru(1)−O(3)	85.5(4)	O(3)−Ru(1)−O(5)	87.1(4)
O(1)−Ru(1)−O(4)	89.6(4)	O(3)−Ru(1)−O(6)	169.0(4)
O(1)−Ru(1)−O(5)	170.4(4)	O(4)−Ru(1)−O(5)	95.7(5)
O(1)−Ru(1)−O(6)	85.4(4)	O(4)−Ru(1)−O(6)	90.5(5)
O(2)−Ru(1)−O(3)	90.3(4)	O(5)−Ru(1)−O(6)	102.5(3)
O(2)−Ru(1)−O(4)	171.0(4)	Ru(1)−O(5)−Ru(1)*	77.9(5)
O(2)−Ru(1)−O(5)	90.1(5)	Ru(1)−O(6)−Ru(1)*	77.0(6)
O(2)−Ru(1)−O(6)	94.9(5)		
Intramolecular Hydrogen Bonds			
O(1)···O(10)	2.80(2)	O(3)···O(8)	2.84(2)
Intermolecular Hydrogen Bonds			
O(7)···O(11)	3.04(2)	O(7)···O(13)	2.94(3)
O(9)···O(12)	2.91(2)		

[a] Symmetry operation: (*) $-x, y, z$.

Cyclic Voltammetry. Cyclic voltammetry for **2**−**4**, **6**, and **7** was performed in DMF solution in a potential range from −2.0

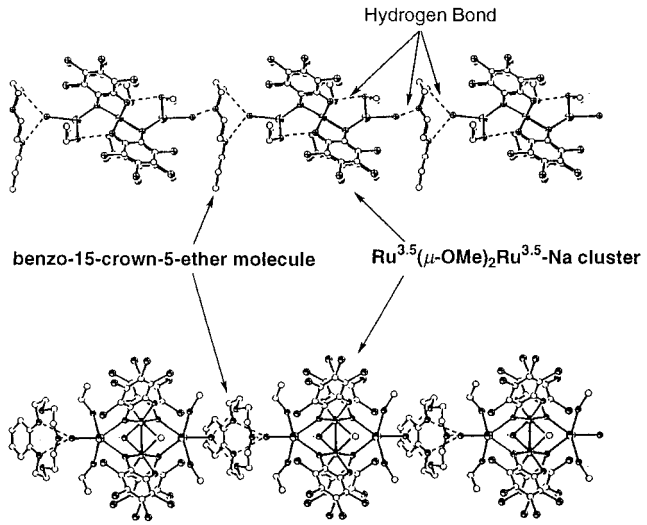

Figure 4. Hydrogen-bonded one-dimensional chain of **5**. The 1-D chain runs along the *b*-axis.

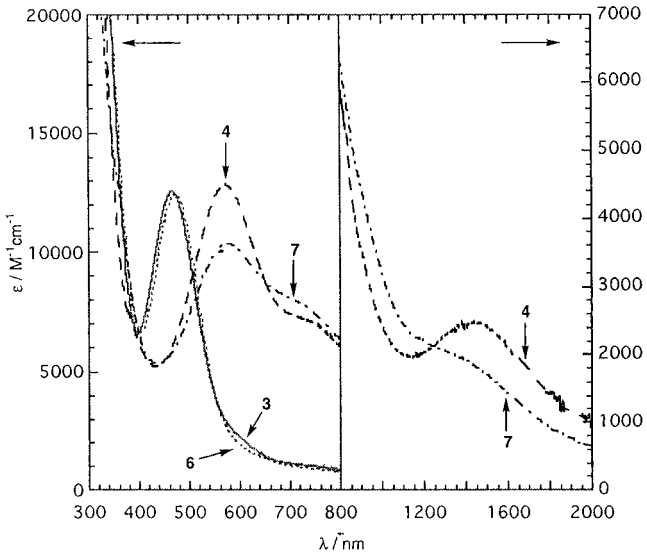

Figure 5. The electronic spectra of the $Ru^{3+}(\mu\text{-}OMe)_2Ru^{3+}$ species **3**, the $Ru^{3.5+}(\mu\text{-}OMe)_2Ru^{3.5+}$ species **4**, the $Ru^{3+}(\mu\text{-}OEt)_2Ru^{3+}$ species **6**, and the $Ru^{3.5+}(\mu\text{-}OEt)_2Ru^{3.5+}$ species **7**, in MeCN under N_2.

Table 4. IR, Electronic Spectral Parameters, Magnetic Moments, and *g* Values Detected from ESR Measurements for **2**−**7**

compd	ν_{C-O}, ν_{C-C}, cm^{-1}	λ_{max}, nm ($\epsilon = M^{-1}\cdot cm^{-1}$ in MeCN)
2	1258, 1436	474 (10300)
3	1254, 1435	470 (12600)
4	1255, 1422	575 (12800), 765 (6900) sh, 1450 (2500) sh
5	1255, 1423	
6	1257, 1435	472 (12500)
7	1255, 1422	575 (10500), 765 (6000) sh, 1400 (2000) sh

compd	magnetic moments, μ_B	ESR, *g* value at 77 K
2	diamagnetic	
3	diamagnetic	
4	1.71 (1.9 K), 2.04 (300 K)	2.54, 2.01, 1.80
5	1.75 (1.9 K), 2.02 (300 K)	2.57, 1.90, 1.73
6	diamagnetic	
7	1.30 (1.9 K), 1.72 (300 K)	2.43, 2.04, 1.86

to +1.0 V vs Ag/AgCl reference electrode. Figure 7 shows the cyclic voltammograms for **3**, **4**, **6**, and **7**. The features of voltammograms for these compounds are essentially identical;

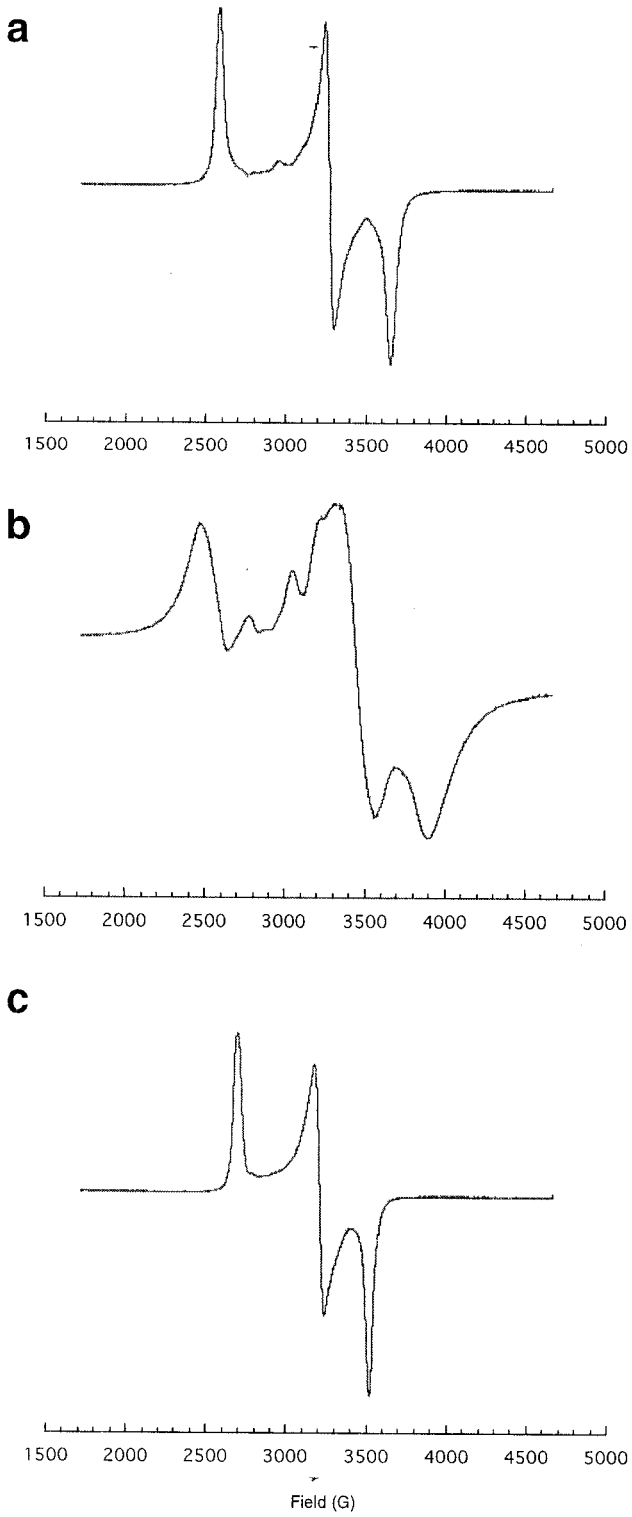

Figure 6. ESR spectra of powder samples of the $Ru^{3.5+}(\mu\text{-}OMe)_2Ru^{3.5+}$ species, (a) **4** and (b) **5**, and the $Ru^{3.5+}(\mu\text{-}OEt)_2Ru^{3.5+}$ species, (c) **7**, which were measured at 77 K (**4**, microwave frequency 9.194 GHz, power 8.03 mW; **5**, microwave frequency 9.196 GHz, power 8.02 mW; and **7**, microwave frequency 9.192 GHz, power 8.03 mW).

two reversible and two quasi-reversible redox waves were clearly observed. Each redox wave was assigned to a metal-origin one-electron process because of assignments of previous work.[18,23] The quasi-reversible wave at $E_{1/2} = -1.58$ V ($I_{pa}/I_{pc} \approx 1$, $\Delta E \geq 70$ mV) arises from the [$Ru^{3+}(\mu\text{-}OR)_2Ru^{3+}/Ru^{2.5+}(\mu\text{-}OR)_2Ru^{2.5+}$] redox couple. The quasi-reversible wave at $E_{1/2} = -0.21$ V ($I_{pa}/I_{pc} \approx 1$, $\Delta E =$ ca. 70 mV) and the reversible wave

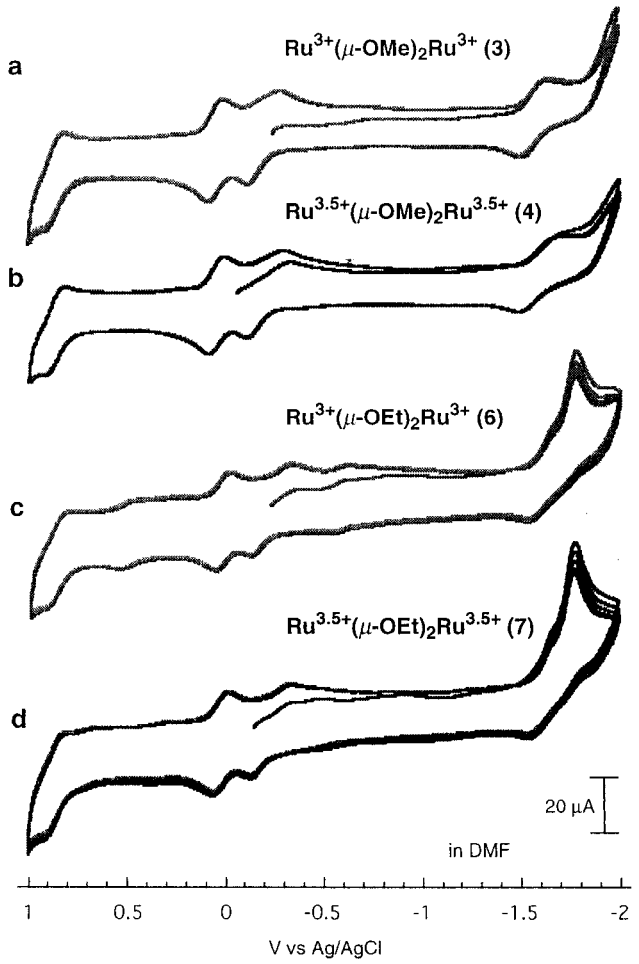

Figure 7. Cyclic voltammograms of (a) the $Ru^{3+}(\mu\text{-}OMe)_2Ru^{3+}$ species **3**, (b) the $Ru^{3.5+}(\mu\text{-}OMe)_2Ru^{3.5+}$ species **4**, (c) the $Ru^{3+}(\mu\text{-}OEt)_2Ru^{3+}$ species **6**, and (d) the $Ru^{3.5+}(\mu\text{-}OEt)_2Ru^{3.5+}$ species **7** in DMF containing $(n\text{-}Bu_4N)ClO_4 = 0.1$ M as a supporting electrolyte. Conditions: [compound] $= 1 \times 10^{-3}$ M; carbon working electrode, Pt counter electrode, and Ag/AgCl reference electrode; under N_2.

at +0.04 V ($I_{pa}/I_{pc} \approx 1$, ΔE = ca. 60 mV) are assigned to the [$Ru^{3.5+}(\mu\text{-}OR)_2Ru^{3.5+}/Ru^{3+}(\mu\text{-}OR)_2Ru^{3+}$] and [$Ru^{4+}(\mu\text{-}OR)_2Ru^{4+}/Ru^{3.5+}(\mu\text{-}OR)_2Ru^{3.5+}$] couples, respectively, on the basis of bulk solution rest potential measurements. The redox potential of [$Ru^{3.5+}(\mu\text{-}OR)_2Ru^{3.5+}/Ru^{3+}(\mu\text{-}OR)_2Ru^{3+}$] is relatively lower, actually, compounds **2**, **3**, and **6** are oxidized gradually in solution (DMF and MeCN) under air. The reversible wave at $E_{1/2} = +0.86$ V ($I_{pa}/I_{pc} \approx 1$, ΔE = ca. 61 mV) could be associated with [$Ru^{4.5+}(\mu\text{-}OR)_2Ru^{4.5+}/Ru^{4+}(\mu\text{-}OR)_2Ru^{4+}$], because the dioxolene ligand-based redox reactions were not detected in these systems including compound **1** and its oxidized compound.[18,23] The similar redox behavior in all compounds indicates that substituents of the bridging ligands exert no significant effect on the electronic states of compounds.

Spectral Investigation of Oxidation and Alcoholysis of 1. Formation of 2−4. The oxidation of **1** in MeOH under air continuously leads to $Ru^{3+}(\mu\text{-}OMe)_2Ru^{3+}$ and $Ru^{3.5+}(\mu\text{-}OMe)_2Ru^{3.5+}$ species. Figure 8 shows the time course of UV−vis spectra of **1** in MeOH under air for 24 h. First, the absorption bands at 480 and 710 nm are observed in MeOH under N_2 atmosphere. This spectrum is accounted for by the formation of axially MeOH coordinated species, $[Ru_2(Cl_4Cat)_4(MeOH)_2]^{3-}$ (**1′**). The absorption band for **1′** does not cross the isosbestic points during the period of oxidation, because it may be due to the rapid oxidation of **1′** to the $Ru^{3+}(\mu\text{-}OMe)_2Ru^{3+}$ species under air. The absorption band at 480 nm changed continuously to the band at ca. 590 nm. These two bands are ascribed to the LMCT bands of **2**−**3** and **4**, respectively. In addition, the observation of isosbestic points at 380 and 537 nm clearly exhibits that the two species $Ru^{3+}(\mu\text{-}OMe)_2Ru^{3+}$ and $Ru^{3.5+}(\mu\text{-}OMe)_2Ru^{3.5+}$ are in equilibrium.

Formation of 6 and 7. In EtOH, both $Ru^{3+}(\mu\text{-}OEt)_2Ru^{3+}$ and $Ru^{3.5+}(\mu\text{-}OEt)_2Ru^{3.5+}$ species are formed by the oxidation and ethanolysis of **1**. The UV−vis spectrum for **1** shows an absorption maximum at 535 nm in EtOH under N_2 atmosphere ($[Ru_2(Cl_4Cat)_4(EtOH)_2]^{3-}$ (**1″**)), with which spectral change by air oxidation was monitored as shown in Figure 9. First, the initial absorption intensity increased slightly and a new absorption band was observed at ca. 500 nm as a shoulder (inset of Figure 9), which shifted finally to 585 nm with isosbestic points at 455 and 558 nm. The absorption bands at 500 and 585 nm correspond to LMCT bands of **6** (472 nm) and **7** (575 nm), respectively. Such spectral variation indicates a continuous conversion from **1″** to **6** and finally to **7** by the air oxidation and structural modification due to ethanolysis. The addition of Ph_4PCl as a countercation leads to the isolation of the $Ru^{3.5+}(\mu\text{-}OEt)_2Ru^{3.5+}$ species **7**, which is the final product of the oxidation reaction.

On the other hand, the air oxidation reaction in the presence of pyrazine (or 2,5-dimethylpyrazine) afforded the $Ru^{3+}(\mu\text{-}OEt)_2Ru^{3+}$ species **6** as a solid. The addition of an excess of pyrazine (or 2,5-dimethylpyrazine) (4 equiv per Ru) to a EtOH solution of **1** under air causes a large shift of the band at 535 nm to 780 nm, which is attributable to the formation of $[Ru(Cl_4Cat)_2(L)_2]^-$ (L = pyrazine (**8**), 2,5-dimethylpyrazine (**9**)) as shown in Figure 10. X-ray crystallographic and several spectroscopic analyses characterized compounds **8** and **9** (Figures S2 and S3 as Supporting Information, showing ORTEP drawings of **8** and **9**, respectively).[24] To confirm the selective conversion from **8** or **9** to the $Ru^{3+}(\mu\text{-}OEt)_2Ru^{3+}$ species by ethanolysis, UV−vis spectral variation was recorded when EtOH was added to a CH_2Cl_2 solution of **9** under air ($EtOH:CH_2Cl_2 = 1:5$ v/v) (Figure 11). The absorption bands at 775 and 600 nm, which are assigned to LMCT and ILCT (interligand charge transfer) bands of **9**, respectively, decrease, and simultaneously, the absorption band at 475 nm increases with an isosbestic point at 517 nm. The increasing absorption peak at 475 nm corresponds to the LMCT band of **6** (472 nm). After 2 h, a final spectrum similar to that of **6** was obtained. On this basis, it is concluded that an equilibrium exists between $[Ru(Cl_4Cat)_2(L)_2]^-$ (**8** and **9**) and the $Ru^{3+}(\mu\text{-}OEt)_2Ru^{3+}$ (**6**) species. The presence of pyrazine derivatives suppresses further oxidation to the $Ru^{3.5+}(\mu\text{-}OEt)_2Ru^{3.5+}$ (**7**) species. Therefore an addition of pyrazine or 2,5-dimethylpyrazine is relevant for the selective isolation of the $Ru^{3+}(\mu\text{-}OEt)_2Ru^{3+}$ species (Scheme 4).

Conclusion

In summary, a series of new edge-sharing bioctahedral $Ru^{3+}(\mu\text{-}OR)_2Ru^{3+}$ and $Ru^{3.5+}(\mu\text{-}OR)_2Ru^{3.5+}$ (R = CH_3 and CH_3CH_2) compounds of tetrachloro-*o*-chatecholate have been

(24) The cyclic voltammetry for **9** was recorded in CH_2Cl_2, but for **8** it failed due to the lower solubility and the occurrence of decomposition of the compound. For **9**, two reversible redox waves, $E_{1/2} = +0.24$ and −0.93 V (vs Ag/AgCl), were observed ($I_{pa}/I_{pc} \approx 1$, $\Delta E = 60-62$ mV). The redox couple at +0.24 V was assigned to the [Ru^{3+}/Ru^{4+}] couple (one-electron transfer). The redox potential $E_{1/2} = -0.93$ V (one-electron transfer) was assigned to the couple of [Ru^{2+}/Ru^{3+}]. The IR spectra for **8** and **9** also showed the characteristic frequencies for catecholate, where the frequencies at 1258 and 1434 cm^{-1} for **8** and at 1257 and 1436 cm^{-1} for **9** were observed.

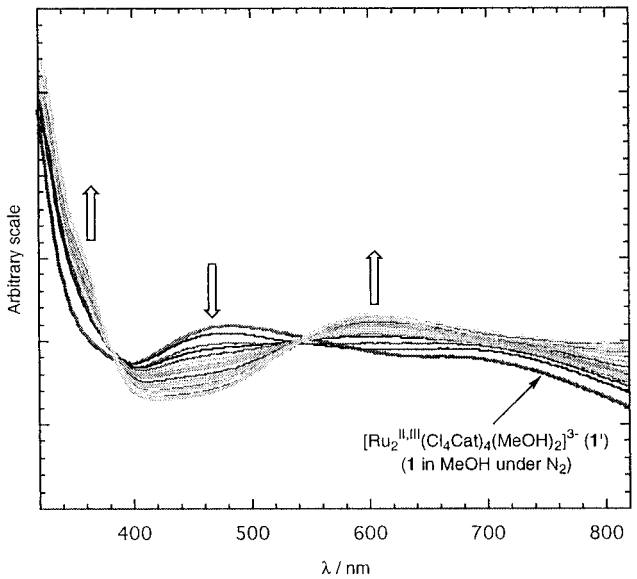

Figure 8. The variation of UV−vis spectra of **1** in MeOH under air.

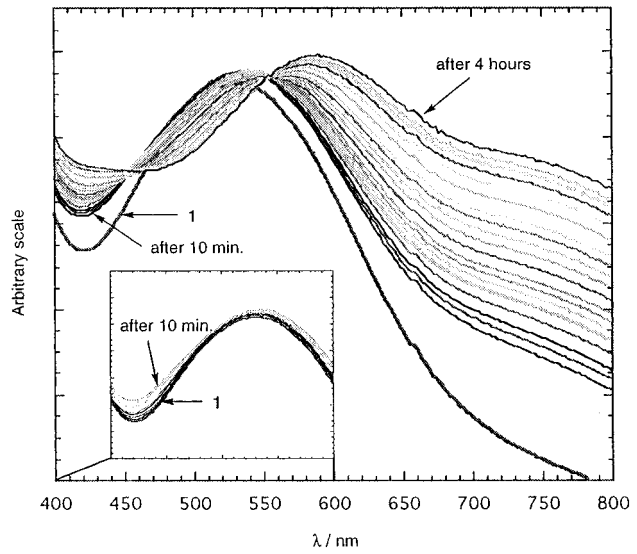

Figure 9. Spectral variation of **1** in EtOH under air. Inset: The variation for the initial 10 min.

synthesized and structurally and physicochemically characterized. The compounds described here are the first example of metal−metal bonded $Ru^{3+}(\mu\text{-}OR)_2Ru^{3+}$ and $Ru^{3.5+}(\mu\text{-}OR)_2Ru^{3.5+}$ compounds in our knowledge.

Crown-ether molecules play an important role in the isolation of labile molecules and intermediates, thus promoting supramolecular complexation.[25] Molecular recognition by the formation of hydrogen bonds affords various specific oligomeric and polymeric molecular assemblies in a solid state arrangement. Namely, the alkaline metal−crown-ether cations behave not only as cations for ionic complexation but also as a crystallization agents by their nature as supramolecular linkers. Their packing effects selectively isolated compounds **3**, **4**, and **5**. In addition, compound **5** was concomitantly obtained as a novel hydrogen-bonded assembly involving a $Ru^{3.5+}(\mu\text{-}OMe)_2Ru^{3.5+}$−Na cluster molecule and free benzo-15-crown-5-ether molecules.

We found that the addition of pyrazine or 2,5-dimethylpyrazine promotes selective isolation of $Ru^{3+}(\mu\text{-}OEt)_2Ru^{3+}$ species. It should be remarked that the details of the mechanism for the

(25) Lehn, J.-M. *Supramolecular Chemistry*; VCH: Weinheim, 1995.

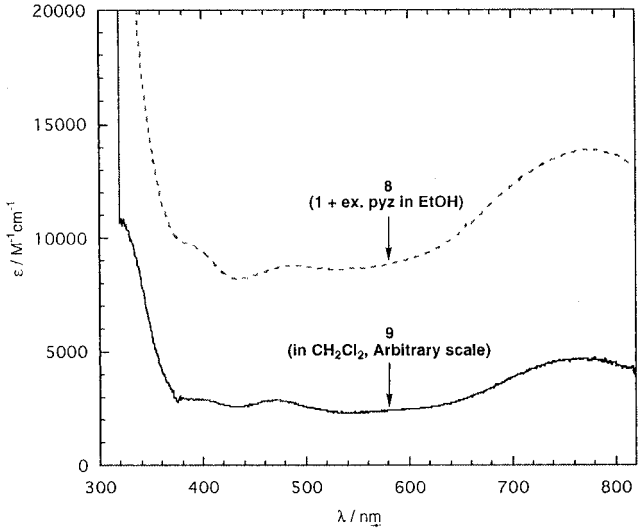

Figure 10. UV−vis spectra of $(Ph_4P)[Ru(Cl_4Cat)_2(Me_2pyz)_2]$ (**9**) (—) in CH_2Cl_2 (under N_2), and a spectrum of EtOH solution of **1** containing an excess of pyrazine under air, exhibiting of the formation of **8** (···).

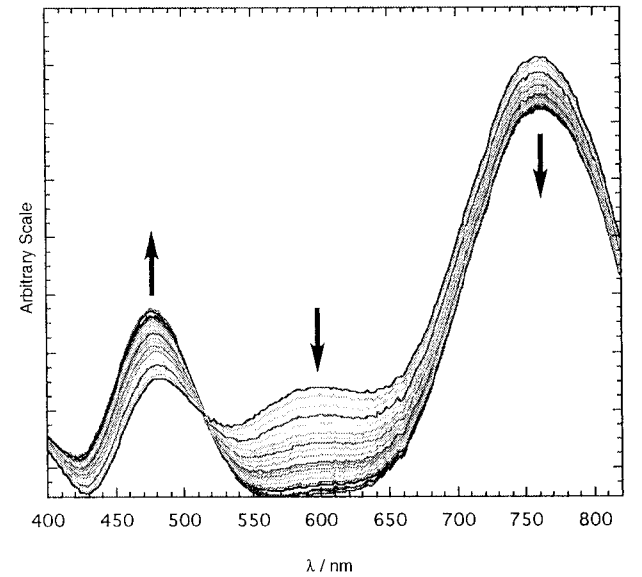

Figure 11. Spectral variation of a CH_2Cl_2 solution of **9** containing EtOH (CH_2Cl_2:EtOH = 5:1 v/v) under air. It was recorded for 2 h and then maintained as such.

structural conversion from the pyrazine-coordinated monoruthenium(III) species to the $Ru^{3+}(\mu\text{-}OR)_2Ru^{3+}$ species are not yet fully understood. Probably, several intermediate species such as $[Ru^{III}(Cl_4Cat)_2]^-$, $[Ru^{III}(Cl_4Cat)_2(EtOH)]^-$, and $[Ru_2^{III,III}(Cl_4Cat)_4(EtOH)_2]^{2-}$ could be presented in this conversion process.

Experimental Section

General Procedures and Materials. All chemicals used for the syntheses were reagent grade. The solvents, MeOH, MeCN, CH_2Cl_2, and DMF, for the spectroscopic measurements were purified by drying and a distillation under N_2. $Na_3[Ru_2(Cl_4Cat)_4(THF)]\cdot 3H_2O\cdot 7THF$ (**1**) was synthesized by the literature method.[18]

Preparation of 2. Compound **2** can be synthesized by method A or method B.

Method A. A MeOH solution (40 cm^3) of **1** (200 mg, 0.14 mmol) was stirred under air for 1 h, where the violet solution changed to a dark blue one. After stirring, solid Ph_4PCl (160 mg, 0.43 mmol) was added, and the solution was stirred further for 5 min and then filtered. The filtrate was allowed to stand in air for 2−3 days to form dark

Scheme 4

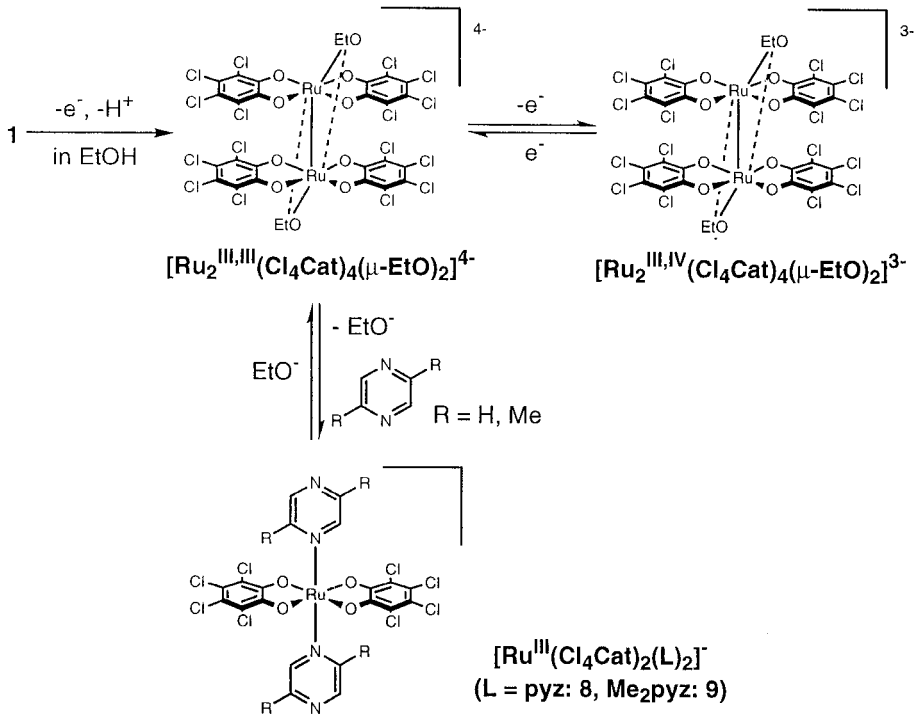

brown prismatic crystals of **2**. They were collected by suction filtration, washed with a minimum amount of 2-propanol, and dried in vacuo.

Method B. The MeOH solution (40 cm^3) of **1** (200 mg, 0.14 mmol) was stirred in air for 30 min and then a solid of Ph_4PCl (160 mg, 0.43 mmol was added). The solution was filtered to remove an insoluble solid, and the filtrate was stirred in air for 2 h. During this time, the brown microcrystals precipitated from dark blue solution. They were collected by suction filtration, washed with a minimum amount of 2-propanol, and dried in vacuo. For **2**: Anal. Calcd for $C_{80}H_{70}Cl_{16}Na_2O_{16}P_2Ru_2$: C, 44.38; H, 3.26. Found: C, 44.32; H, 3.07. UV−vis (λ_{max}/nm ($\epsilon/M^{-1}\cdot cm^{-1}$) in MeCN): 474 (10300). IR (cm^{-1}) on KBr: ν(C−O), 1258; ν(C═C), 1436. Diamagnetic.

Preparation of 3. Compound **3** can be synthesized by method A or method B. The single crystal for X-ray crystallographic analysis was prepared by method A.

Method A. A MeOH solution (40 cm^3) of **1** (200 mg, 0.14 mmol) was stirred under air for 1 h, where the violet solution changed to a dark blue one. After stirring, solid dibenzo-18-crown-6-ether (180 mg, 0.5 mmol) was added, and the solution was stirred further for 10 min. In this time, an excess amount of dibenzo-18-crown-6-ether remained as a white solid in solution. The mixture was filtered to remove an excess of dibenzo-18-crown-6-ether, and the filtrate was allowed to stand in air for 2−3 days to form brown prismatic crystals of **3**. A single crystal was suitable for X-ray crystallographic analysis.

Method B. A MeOH solution (40 cm^3) of **1** (200 mg, 0.14 mmol) was stirred under air for 30 min, and then a solid of dibenzo-18-crown-6-ether (160 mg, 0.44 mmol) was added. After stirring for 10 min, the solution was filtered to remove an insoluble solid (free dibenzo-18-crown-6-ether) and the filtration was stirred for 2 h. During this time, bright brown microcrystals precipitated from dark blue solution. They were collected by suction filtration, washed with a minimum amount of 2-propanol, and dried in vacuo. For **3**: Anal. Calcd for $C_{74}H_{90}Cl_{16}Na_4O_{32}Ru_2$: C, 37.77; H, 3.86. Found: C, 37.46; H, 3.13. UV−vis (λ_{max}/nm ($\epsilon/M^{-1}\cdot cm^{-1}$) in MeCN): 470 (12600). IR (cm^{-1}) on KBr: ν(C−O), 1254; ν(C═C), 1435. Diamagnetic.

Preparation of 4. A MeOH solution (40 cm^3) of **1** (200 mg, 0.14 mmol) was stirred under air for 1 h. After stirring, solid benzo-15-crown-5-ether (120 mg, 0.45 mmol) was added, and the solution was stirred further for 5 min and then filtered. The filtrate was allowed to in air for 2−3 days to form dark blue prismatic crystals of **4**. A single crystal was suitable for X-ray crystallographic analysis. The crystals were collected by suction filtration, washed with a minimum amount of 2-propanol, and dried in vacuo. For **4**: Anal. Calcd for $C_{60}H_{70}Cl_{16}Na_3O_{26}Ru_2$: C, 35.23; H, 3.45. Found: C, 34.62; H, 2.75. UV−vis (λ_{max}/nm ($\epsilon/M^{-1}\cdot cm^{-1}$) in MeCN): 575 (12800), 765 (6900, shoulder), 1450 (2500). IR (cm^{-1}) on KBr: ν(C−O), 1255; ν(C═C), 1422. μ_{eff} = 1.71 (1.9 K) and 2.04 μ_B (300 K).

Preparation of 5. A MeOH solution (30 cm^3) of **1** (200 mg, 0.14 mmol) was stirred under air for 1 h. After stirring, a solid of benzo-15-crown-5-ether (150 mg, 0.56 mmol) was added, and the solution was stirred further for 5 min. To this MeOH solution was added 30 cm^3 of EtOH, and then the solution was filtered. The filtrate was allowed to stand for in air for 2−3 days to form dark blue prismatic crystals of **5**. A single crystal was suitable for X-ray crystallographic analysis. The crystals were collected by suction filtration, washed with a minimum amount of 2-propanol, and dried in vacuo. For **5**: Anal. Calcd for $C_{60}H_{72}Cl_{16}Na_3O_{27}Ru_2$: C, 34.92; H, 3.52. Found: C, 35.31; H, 3.62. IR (cm^{-1}) on KBr: ν(C−O), 1255; ν(C═C), 1423. μ_{eff} = 1.75(1.9 K) and 2.02 μ_B (300 K).

Preparation of 6. An EtOH solution (30 cm^3) of **1** (200 mg, 0.14 mmol) was stirred under air for 1 h. Then, an excess amount of pyrazine (50 mg, 0.62 mmol) was added into this solution. The solution changed to greenish blue, and this solution was stirred under air for 1 h. Solid Ph_4PCl (160 mg, 0.43 mmol) was added, and the solution was stirred further for 5 min and then filtered. The filtrate was allowed to stand in air for 2−3 days to form dark blue prismatic crystals of **6**. A single crystal was suitable for X-ray crystallographic analysis. The crystals were collected by suction filtration, washed with a minimum amount of 2-propanol, and dried in vacuo. The use of 2,5-dimethylpyrazine (70 mg, 0.65 mmol) instead of pyrazine also afforded a crystalline sample of **6**. For **6**: Anal. Calcd for $C_{80}H_{70}Cl_{16}Na_2O_{16}P_2Ru_2$: C, 44.38; H, 3.26. Found: C, 44.03; H, 3.21. UV−vis (λ_{max}/nm ($\epsilon/M^{-1}\cdot cm^{-1}$) in MeCN): 472 (12500). IR (cm^{-1}) on KBr: ν(C−O), 1257; ν(C═C), 1435. Diamagnetic.

Preparation of 7. An EtOH solution (30 cm^3) of **1** (200 mg, 0.14 mmol) was stirred under air for 1 h. Then, solid Ph_4PCl (160 mg, 0.43 mmol) was added, and the solution was stirred further for 5 min and then filtered. The filtrate was allowed to stand in air for 2−3 days to form dark blue prismatic crystals of **7**. They were collected by suction filtration, washed with a minimum amount of 2-propanol, and dried in vacuo. For **7**: Anal. Calcd for $C_{64}H_{66}Cl_{16}Na_2O_{16}P_1Ru_2$: C, 39.67; H,

Table 5. Crystallographic Data for **3**−**6**

	3	**4**	**5**	**6**
formula	$C_{74}H_{90}O_{32}Cl_{16}Ru_2Na_4$	$C_{61}H_{74}O_{27}Cl_{16}Ru_2Na_3$	$C_{60}H_{72}O_{27}Cl_{16}Ru_2Na_3$	$C_{80}H_{70}O_{16}Cl_{16}Ru_2P_2Na_2$
fw	2350.84	2077.60	2063.57	2164.74
cryst syst	monoclinic	triclinic	orthorhombic	monoclinic
space group	*C*2/*m* (No. 12)	$P\bar{1}$ (No. 2)	*Cmc*2_1 (No. 36)	$P2_1/n$ (No. 14)
T/ °C	−100 ± 1	−100 ± 1	−100 ± 1	−100 ± 1
λ/Å	0.71069	0.71069	0.71069	0.71069
a/Å	19.511(3)	12.657(1)	21.6069(3)	12.9343(8)
b/Å	18.803(2)	16.5820(5)	15.769(1)	26.275(2)
c/Å	14.1254(3)	20.887(2)	24.4792(4)	15.3341(5)
α/deg	90	76.303(2)	90	90
β/deg	111.0893(5)	87.1994(8)	90	114.004(1)
γ/deg	90	80.4219(7)	90	90
V/Å^3	4835.1(8)	4199.3(5)	8340.7(7)	4760.6(4)
Z	2	2	4	2
D_{calcd}/g·cm^{-3}	1.615	1.643	1.643	1.510
μ(Mo Kα)/cm^{-1}	8.49	9.56	9.63	8.67
no. of reflns	4226 ($I > 3.00\sigma(I)$)	14345 ($I > 3.00\sigma(I)$)	4248 ($I > 2.00\sigma(I)$)	3899 ($I > 3.00\sigma(I)$)
p-factor	0.05	0.02	0.05	0.05
R^a	0.045	0.061	0.098	0.088
$R_w{}^{b,c}$	0.083	0.087	0.103	0.110

[a] $R = \sum||F_o| - |F_c||/\sum|F_o|$. [b] $R_w = [\sum w(|F_o| - |F_c|)^2/\sum w|F_o|^2]^{1/2}$. [c] $w = 1/[\sigma^2(F_o) + p^2|F_o|^2/4]$.

3.43. Found: C, 40.39; H, 3.14. UV−vis (λ_{max}/nm (ϵ/M^{-1}·cm^{-1}) in MeCN): 575 (10500), 765 (∼6000, shoulder), 1400 (∼2000, shoulder). IR (cm^{-1}) on KBr: ν(C−O), 1255; ν(C═C), 1422. μ_{eff} = 1.30 (1.9 K) and 1.72 μ_B (300 K).

Physical Measurements. Infrared spectra were measured on KBr disks with a Perkin-Elmer System 2000 FT-IR spectrophotometer. UV−vis−near-IR spectra were recorded with a Hewlett-Packard 8452A diode array spectrophotometer and a Hitachi U-3500 spectrophotometer. General magnetic susceptibility data were measured over the temperature range 2.0−300 K using an MPMS5 SQUID susceptometer (Quantum Design, Inc.) interfaced with an HP Vectra computer system, where the applied magnetic fields were 1 T. The samples for magnetic measurements were ground to powder in order to avoid an effect of the anisotropy from crystal orientation. Corrections were applied for diamagnetism using Pascal's constants[26] and for aluminum foil and vinyl capsule wrapping samples. Effective magnetic moments were calculated by the equation $\mu_{eff} = 2.828(\chi_M T)^{1/2}$, where χ_M is the magnetic susceptibility per formula unit. Cyclic voltammograms were recorded in DMF (tetrabutylammonium perchlorate [$(NBu_4)ClO_4$] = 0.1 M as a supporting electrolyte) under nitrogen atmosphere with BAS 100B/W(CV-50W). At the beginning of measurement for the compounds, CV's of DMF and CH_2Cl_2 with only supporting electrolyte were measured. To this solution were added the compounds ([compound] = 1 × 10^{-3} M for **2**−**4**, **6**, and **7**, 1 × 10^{-4} M for **9**) and measured with a unit of carbon working electrode, Pt counter electrode, and Ag/AgCl reference electrode.

X-ray Data Collection, Reduction, and Structure Determination. Single crystals of **3**−**6**, **8**, and **9** were prepared by the each method described in the synthetic procedure. All single crystals for the crystallographic analysis were cut from a thin plate crystal and mounted on a glass rod. Measurements were made on a Rigaku Mercury CCD diffractometer with graphite-monochromated Mo Kα radiation (λ = 0.71069 Å). The data were collected at a temperature of −100 ± 1 °C. An empirical absorption correction based on azimuthal scans of several reflections was applied. The structures were solved by direct methods[27] and expanded using Fourier techniques.[28] Except for compound **5**, the non-hydrogen atoms were refined anisotropically, while hydrogen atoms were refined isotropically. The refinement of all atoms for **5** was done with isotropically because of the lack of reflections. Full-matrix least-squares refinements based on 4226 (**3**), 14345 (**4**), 4248 (**5**), 3899 (**6**), 8458 (**8**), and 3727 (**9**) ($I > 3.00\sigma(I)$, except ($I > 2.00\sigma(I)$) for **5**) observed reflections were employed, where the unweighted and weighted agreement factors of $R = \sum||F_o| - |F_c||/\sum|F_o|$ and $R_w = [\sum w(|F_o| - |F_c|)_2/\sum w|F_o|^2]^{1/2}$ were used. The weighting scheme was based on counting statistics. Plots of $\sum w(|F_o| - |F_c|)^2$ versus $|F_o|$, reflection order in data collection, $\sin\theta/\lambda$, and various classes of indices showed no unusual trends. Neutral atomic scattering factors were taken from Cromer and Waber.[29] Anomalous dispersion effects were included in Fcalcd; the values $\Delta f'$ and $\Delta f''$ were those of Creagh and McAuley.[30] The values for the mass attenuation coefficients are those of Creagh and Hubbel.[31] All calculations were performed using the teXsan crystallographic software package of Molecular Structure Corporation.[32] Although X-ray crystallographic analyses were performed at low temperature, the fragility of the crystals and the existence of disordering made it difficult to improve the quality of the X-ray crystallographic analysis for **4** and **6**. For compound **5**, the lack of reflections and isotropical refinement made it difficult to improve the quality of the X-ray crystallographic analysis. The crystal data and details of the structure determinations for **3**−**6** are summarized in Table 5.

Acknowledgment. This work was supported by a Grant-In-Aid for Scientific Research from the Japanese Ministry of Education Science, Sports, and Culture. H.M. is grateful to the JSPS Research Fellowships for Young Scientists. We also acknowledge Professor Takashi Kawamura in Gifu University for helpful discussion in ESR measurements.

Supporting Information Available: X-ray crystallographic files in CIF format for the structure determinations of **3**−**6**, **8**, and **9**. Figures S1−S3, showing the ORTEP drawings of **6**, **8**, and **9**, respectively. This material is available free of charge via the Internet at http://pubs.acs.org.

IC0010252

(26) Boudreaux, E. A.; Mulay, L. N. *Theory and Applications of Molecular Paramagnetism*; John Wiley and Sons: New York, 1976; pp 491−495.

(27) (a) SIR92: Altomare, A.; Burla, M. C.; Camalli, M.; Cascarano, M.; Giacovazzo, C.; Guagliardi, A.; Polidori, G. *J. Appl. Crystallogr.* **1994**, *27*, 435. (b) PATTY: Beurskens, P. T.; Admiraal, G.; Beurskens, G.; Bosman, W. P.; Garcia-Granda, S.; Gould, R. O.; Smits, J. M. M.; Smykalla, C. (1992).

(28) DIRDIF94: Beurskens, P. T.; Admiraal, G.; Beurskens, G.; Bosman, W. P.; de Gelder, R.; Israel, R.; Smits, J. M. M. The DIRDIF program system. Technical Report of the Crystallography Laboratory; University of Nijmegen: The Netherlands, 1994.

(29) Cromer, D. T.; Waber, J. T. *International Tables for Crystallography*; The Kynoch Press: Birmingham, England, 1974; Vol. IV, Table 2.2A.

(30) Creagh, D. C.; McAuley, W. J. In *International Tables for Crystallography*; Wilson, A. J. C., Ed.; Kluwer Academic Publishers: Boston, 1992; Vol. C, Table 4.2.6.8, pp 219−222.

(31) Creagh, D. C.; Hubbell, J. H. In *International Tables for Crystallography*; Wilson, A. J. C., Ed.; Kluwer Academic Publishers: Boston, 1992; Vol. C, Table 4.2.4.3, pp 200−206.

(32) teXsan: Crystal Structure Analysis Package, Molecular Structure Corporation (1985 and 1992).